

Measurement of the $e^+e^- \rightarrow \pi^+\pi^-J/\psi$ cross section in the vicinity of 3.872 GeV

M. Ablikim¹, M. N. Achasov^{11,b}, P. Adlarson⁷⁰, M. Albrecht⁴, R. Aliberti³¹, A. Amoroso^{69A,69C}, M. R. An³⁵, Q. An^{66,53}, X. H. Bai⁶¹, Y. Bai⁵², O. Bakina³², R. Baldini Ferroli^{26A}, I. Balossino^{1,27A}, Y. Ban^{42,g}, V. Batzskaya^{1,40}, D. Becker³¹, K. Begzsuren²⁹, N. Berger³¹, M. Bertani^{26A}, D. Bettoni^{27A}, F. Bianchi^{69A,69C}, J. Bloms⁶³, A. Bortone^{69A,69C}, I. Boyko³², R. A. Briere⁵, A. Brueggemann⁶³, H. Cai⁷¹, X. Cai^{1,53}, A. Calcaterra^{26A}, G. F. Cao^{1,58}, N. Cao^{1,58}, S. A. Cetin^{57A}, J. F. Chang^{1,53}, W. L. Chang^{1,58}, G. Chelkov^{32,a}, C. Chen³⁹, Chao Chen⁵⁰, G. Chen¹, H. S. Chen^{1,58}, M. L. Chen^{1,53}, S. J. Chen³⁸, S. M. Chen⁵⁶, T. Chen¹, X. R. Chen^{28,58}, X. T. Chen¹, Y. B. Chen^{1,53}, Z. J. Chen^{23,h}, W. S. Cheng^{69C}, S. K. Choi⁵⁰, X. Chu³⁹, G. Cibinetto^{27A}, F. Cossio^{69C}, J. J. Cui⁴⁵, H. L. Dai^{1,53}, J. P. Dai⁷³, A. Dbeyssi¹⁷, R. E. de Boer⁴, D. Dedovich³², Z. Y. Deng¹, A. Denig³¹, I. Denysenko³², M. Destefanis^{69A,69C}, F. De Mori^{69A,69C}, Y. Ding³⁶, J. Dong^{1,53}, L. Y. Dong^{1,58}, M. Y. Dong^{1,53,58}, X. Dong⁷¹, S. X. Du⁷⁵, P. Egorov^{32,a}, Y. L. Fan⁷¹, J. Fang^{1,53}, S. S. Fang^{1,58}, W. X. Fang¹, Y. Fang¹, R. Farinelli^{27A}, L. Fava^{69B,69C}, F. Feldbauer⁴, G. Felici^{26A}, C. Q. Feng^{66,53}, J. H. Feng⁵⁴, K. Fischer⁶⁴, M. Fritsch⁴, C. Fritsch⁶³, C. D. Fu¹, H. Gao⁵⁸, Y. N. Gao^{42,g}, Yang Gao^{66,53}, S. Garbolino^{69C}, I. Garzia^{27A,27B}, P. T. Ge⁷¹, Z. W. Ge³⁸, C. Geng⁵⁴, E. M. Gersabeck⁶², A. Gilman⁶⁴, K. Goetzen¹², L. Gong³⁶, W. X. Gong^{1,53}, W. Gradl³¹, M. Greco^{69A,69C}, L. M. Gu³⁸, M. H. Gu^{1,53}, Y. T. Gu¹⁴, C. Y. Guan^{1,58}, A. Q. Guo^{28,58}, L. B. Guo³⁷, R. P. Guo⁴⁴, Y. P. Guo^{10,f}, A. Guskov^{32,a}, T. T. Han⁴⁵, W. Y. Han³⁵, X. Q. Hao¹⁸, F. A. Harris⁶⁰, K. K. He⁵⁰, K. L. He^{1,58}, F. H. Heinsius⁴, C. H. Heinz³¹, Y. K. Heng^{1,53,58}, C. Herold⁵⁵, Himmelreich³¹, G. Y. Hou^{1,58}, Y. R. Hou⁵⁸, Z. L. Hou¹, H. M. Hu^{1,58}, J. F. Hu^{51,i}, Z. Hu^{1,53,58}, Y. Hu¹, G. S. Huang^{66,53}, K. X. Huang⁵⁴, L. Q. Huang⁶⁷, L. Q. Huang^{28,58}, X. T. Huang⁴⁵, Y. P. Huang¹, Z. Huang^{42,g}, T. Hussain⁶⁸, N. Hüskens^{25,31}, W. Imoehi²⁵, M. Irshad^{66,53}, J. Jackson²⁵, S. Jaeger³⁶, S. Janchiv²⁹, E. Jang⁵⁰, J. H. Jeong⁵⁰, Q. Ji¹, Q. P. Ji¹⁸, X. B. Ji^{1,58}, X. L. Ji^{1,53}, Y. Y. Ji⁴⁵, Z. K. Jia^{66,53}, H. B. Jiang⁴⁵, S. S. Jiang³⁵, X. S. Jiang^{1,53,58}, Y. Jiang⁵⁸, J. B. Jiao⁴⁵, Z. Jiao²¹, S. Jin³⁸, Y. Jin⁶¹, M. Q. Jing^{1,58}, T. Johansson⁷⁰, N. Kalantar-Nayestanaki⁵⁹, X. S. Kang³⁶, R. Kappert⁵⁹, M. Kavatsyuk⁵⁹, B. C. Ke⁷⁵, I. K. Keshk⁴, A. Khoukaz⁶³, P. Kiese³¹, R. Kiuchi¹, R. Kliemt¹², L. Koch³³, O. B. Kolcu^{57A}, B. Kopf⁴, M. Kuemmel⁴, M. Kuessner⁴, A. Kupsc^{40,70}, W. Kühn³³, J. J. Lane⁶², J. S. Lange³³, P. Larin¹⁷, A. Lavania²⁴, L. Lavezzi^{69A,69C}, Z. H. Lei^{66,53}, H. Leithoff³¹, M. Lellmann³¹, T. Lenz³¹, C. Li⁴³, C. Li³⁹, C. H. Li³⁵, Cheng Li^{66,53}, D. M. Li⁷⁵, F. Li^{1,53}, G. Li¹, H. Li⁴⁷, H. Li^{66,53}, H. B. Li^{1,58}, H. J. Li¹⁸, H. N. Li^{51,i}, J. Q. Li⁴, J. S. Li⁵⁴, J. W. Li⁴⁵, Ke Li¹, L. J. Li¹, L. K. Li¹, Lei Li³, M. H. Li³⁹, P. R. Li^{34,j,k}, S. X. Li¹⁰, S. Y. Li⁵⁶, T. Li⁴⁵, W. D. Li^{1,58}, W. G. Li¹, X. H. Li^{66,53}, X. L. Li⁴⁵, Xiaoyu Li^{1,58}, H. Liang^{66,53}, H. Liang^{1,58}, H. Liang³⁰, Y. F. Liang⁴⁹, Y. T. Liang^{28,58}, G. R. Liao¹³, L. Z. Liao⁴⁵, J. Libby²⁴, A. Limphirat⁵⁵, C. X. Lin⁵⁴, D. X. Lin^{28,58}, T. Lin¹, B. J. Liu¹, C. X. Liu¹, D. Liu^{17,66}, F. H. Liu⁴⁸, Fang Liu¹, Feng Liu⁶, G. M. Liu^{51,i}, H. Liu^{34,j,k}, H. B. Liu¹⁴, H. M. Liu^{1,58}, Huanhuan Liu¹, Huihui Liu¹⁹, J. B. Liu^{66,53}, J. L. Liu⁶⁷, J. Y. Liu^{1,58}, K. Liu¹, K. Y. Liu³⁶, Ke Liu²⁰, L. Liu^{66,53}, Lu Liu³⁹, M. H. Liu^{10,f}, P. L. Liu¹, Q. Liu⁵⁸, S. B. Liu^{66,53}, T. Liu^{10,f}, W. K. Liu³⁹, W. M. Liu^{66,53}, X. Liu^{34,j,k}, Y. Liu^{34,j,k}, Y. B. Liu³⁹, Z. A. Liu^{1,53,58}, Z. Q. Liu⁴⁵, X. C. Lou^{1,53,58}, F. X. Lu⁵⁴, H. J. Lu²¹, J. G. Lu^{1,53}, X. L. Lu¹, Y. Lu⁷, Y. P. Lu^{1,53}, Z. H. Lu¹, C. L. Luo³⁷, M. X. Luo⁷⁴, T. Luo^{10,f}, X. L. Luo^{1,53}, X. R. Lyu⁵⁸, Y. F. Lyu³⁹, F. C. Ma³⁶, H. L. Ma¹, L. L. Ma⁴⁵, M. M. Ma^{1,58}, Q. M. Ma¹, R. Q. Ma^{1,58}, R. T. Ma⁵⁸, X. Y. Ma^{1,53}, Y. Ma^{42,g}, F. E. Maas¹⁷, M. Maggiora^{69A,69C}, S. Maldaner⁴, S. Malde⁶⁴, Q. A. Malik⁶⁸, A. Mangoni^{26B}, Y. J. Mao^{42,g,g}, Z. P. Mao¹, S. Marcello^{69A,69C}, Z. X. Meng⁶¹, J. G. Messchendorp^{59,12}, G. Mezzadri^{1,27A}, H. Miao¹, T. J. Min³⁸, R. E. Mitchell²⁵, X. H. Mo^{1,53,58}, N. Yu. Muchnoi^{11,b}, Y. Nefedov³², F. Nerling^{17,d}, I. B. Nikolaev¹¹, Z. Ning^{1,53}, S. Nisar^{9,l}, Y. Niu⁴⁵, S. L. Olsen⁵⁸, Q. Ouyang^{1,53,58}, S. Pacetti^{26B,26C}, X. Pan^{10,f}, Y. Pan⁵², A. Pathak¹, A. Pathak³⁰, M. Pelizaeus⁴, H. P. Peng^{66,53}, K. Peters^{12,d}, J. Pettersson⁷⁰, J. L. Ping³⁷, R. G. Ping^{1,58}, S. Plura³¹, S. Pogodin³², V. Prasad^{66,53}, F. Z. Qi¹, H. Qi^{66,53}, H. R. Qi⁵⁶, M. Qi³⁸, T. Y. Qi^{10,f}, S. Qian^{1,53}, W. B. Qian⁵⁸, Z. Qian⁵⁴, C. F. Qiao⁵⁸, J. J. Qin⁶⁷, L. Q. Qin¹³, X. P. Qin^{10,f}, X. S. Qin⁴⁵, Z. H. Qin^{1,53}, J. F. Qiu¹, S. Q. Qu³⁹, S. Q. Qu⁵⁶, K. H. Rashid⁶⁸, C. F. Redmer³¹, K. J. Ren³⁵, A. Rivetti^{69C}, V. Rodin⁵⁹, M. Rolo^{69C}, G. Rong^{1,58}, Ch. Rosner¹⁷, S. N. Ruan³⁹, H. S. Sang⁶⁶, A. Sarantsev^{32,c}, Y. Schelhaas³¹, C. Schnier⁴, K. Schönning⁷⁰, M. Scodeggio^{27A,27B}, K. Y. Shan^{10,f}, Y. Shan²², X. Y. Shan^{66,53}, J. F. Shangguan⁵⁰, L. G. Shao^{1,58}, M. Shao^{66,53}, C. P. Shen^{10,f}, H. F. Shen^{1,58}, X. Y. Shen^{1,58}, B. A. Shi⁵⁸, H. C. Shi^{66,53}, J. Y. Shi¹, q. q. Shi⁵⁰, R. S. Shi^{1,58}, X. Shi^{1,53}, X. D. Shi^{66,53}, J. J. Song¹⁸, W. M. Song^{1,30}, Y. X. Song^{42,g}, S. Sosio^{69A,69C}, S. Spataro^{69A,69C}, F. Stieler³¹, K. X. Su⁷¹, P. P. Su⁵⁰, Y. J. Su⁵⁸, G. X. Sun¹, H. Sun⁵⁸, H. K. Sun¹, J. F. Sun¹⁸, L. Sun⁷¹, S. S. Sun^{1,58}, T. Sun^{1,58}, W. Y. Sun³⁰, X. Sun^{23,h}, Y. J. Sun^{66,53}, Y. Z. Sun¹, Z. T. Sun⁴⁵, Y. H. Tan⁷¹, Y. X. Tan^{66,53}, C. J. Tang⁴⁹, G. Y. Tang¹, J. Tang⁵⁴, L. Y. Tao⁶⁷, Q. T. Tao^{23,h}, M. Tat⁶⁴, J. X. Teng^{66,53}, V. Thoren⁷⁰, W. H. Tian⁴⁷, Y. Tian^{28,58}, I. Uman^{57B}, B. Wang¹, B. L. Wang⁵⁸, C. W. Wang³⁸, D. Y. Wang^{42,g}, F. Wang⁶⁷, H. J. Wang^{34,j,k}, H. P. Wang^{1,58}, K. Wang^{1,53}, L. L. Wang¹, M. Wang⁴⁵, M. Z. Wang^{42,g}, Meng Wang^{1,58}, S. Wang¹³, S. Wang^{10,f}, T. Wang^{10,f}, T. J. Wang³⁹, W. Wang⁵⁴, W. H. Wang⁷¹, W. P. Wang^{66,53}, X. Wang^{42,g}, X. F. Wang^{34,j,k}, X. L. Wang^{10,f}, Y. D. Wang⁴¹, Y. F. Wang^{1,53,58}, Y. H. Wang⁴³, Y. Q. Wang¹, Yaqian Wang^{1,16}, Y. Wang⁵⁶, Z. Wang^{1,53}, Z. Y. Wang^{1,58}, Ziyi Wang⁵⁸, D. H. Wei¹³, F. Weidner⁶³, S. P. Wen¹, D. J. White⁶², U. Wiedner⁴, G. Wilkinson⁶⁴, M. Wolke⁷⁰, L. Wollenberg⁴, J. F. Wu^{1,58}, L. H. Wu¹, L. J. Wu^{1,58}, X. Wu^{10,f}, X. H. Wu³⁰, Y. Wu⁶⁶, Z. Wu^{1,53}, L. Xia^{66,53}, T. Xiang^{42,g}, D. Xiao^{34,j,k}, G. Y. Xiao³⁸, H. Xiao^{10,f}, S. Y. Xiao¹, Y. L. Xiao^{10,f}, Z. J. Xiao³⁷, C. Xie³⁸, X. H. Xie^{42,g}, Y. Xie⁴⁵, Y. G. Xie^{1,53}, Y. H. Xie⁶, Z. P. Xie^{66,53}, T. Y. Xing^{1,58}, C. F. Xu¹, C. J. Xu⁵⁴, G. F. Xu¹, H. Y. Xu⁶¹, Q. J. Xu¹⁵, X. P. Xu⁵⁰, Y. C. Xu⁵⁸, Z. P. Xu³⁸, F. Yan^{10,f}, L. Yan^{10,f}, W. B. Yan^{66,53}, W. C. Yan⁷⁵, H. J. Yang^{46,e}, H. L. Yang³⁰, H. X. Yang¹, L. Yang⁴⁷, S. L. Yang⁵⁸, Tao Yang¹, Y. F. Yang³⁹, Y. X. Yang^{1,58}, Yifan Yang^{1,58}, M. Ye^{1,53}, M. H. Ye⁸, J. H. Yin¹, Z. Y. You⁵⁴, B. X. Yu^{1,53,58}, C. X. Yu³⁹, G. Yu^{1,58}, T. Yu⁶⁷, X. D. Yu^{42,g}, C. Z. Yuan^{1,58}, L. Yuan², S. C. Yuan¹, X. Q. Yuan¹, Y. Yuan^{1,58}, Z. Y. Yuan⁵⁴, C. X. Yue³⁵, A. A. Zafar⁶⁸, F. R. Zeng⁴⁵, X. Zeng⁶, Y. Zeng^{23,h}, Y. H. Zhan⁵⁴, A. Q. Zhang¹, B. L. Zhang¹, B. X. Zhang¹, D. H. Zhang³⁹, G. Y. Zhang¹⁸, H. Zhang⁶⁶, H. H. Zhang⁵⁴, H. H. Zhang³⁰, H. Y. Zhang^{1,53}, J. L. Zhang⁷², J. Q. Zhang³⁷, J. W. Zhang^{1,53,58}, J. X. Zhang^{34,j,k}, J. Y. Zhang¹, J. Z. Zhang^{1,58}, Jianyu Zhang^{1,58}, Jiawei Zhang^{1,58}, L. M. Zhang⁵⁶, L. Q. Zhang⁵⁴, Lei Zhang³⁸, P. Zhang¹, Q. Y. Zhang^{35,75}, Shuihan Zhang^{1,58}, Shulei Zhang^{23,h}, X. D. Zhang⁴¹, X. M. Zhang¹,

X. Y. Zhang⁴⁵, X. Y. Zhang⁵⁰, Y. Zhang⁶⁴, Y. T. Zhang⁷⁵, Y. H. Zhang^{1,53}, Yan Zhang^{66,53}, Yao Zhang¹, Z. H. Zhang¹, Z. Y. Zhang⁷¹, Z. Y. Zhang³⁹, G. Zhao¹, J. Zhao³⁵, J. Y. Zhao^{1,58}, J. Z. Zhao^{1,53}, Lei Zhao^{66,53}, Ling Zhao¹, M. G. Zhao³⁹, Q. Zhao¹, S. J. Zhao⁷⁵, Y. B. Zhao^{1,53}, Y. X. Zhao^{28,58}, Z. G. Zhao^{66,53}, A. Zhemchugov^{32,a}, B. Zheng⁶⁷, J. P. Zheng^{1,53}, Y. H. Zheng⁵⁸, B. Zhong³⁷, C. Zhong⁶⁷, X. Zhong⁵⁴, H. Zhou⁴⁵, L. P. Zhou^{1,58}, X. Zhou⁷¹, X. K. Zhou⁵⁸, X. R. Zhou^{66,53}, X. Y. Zhou³⁵, Y. Z. Zhou^{10,f}, J. Zhu³⁹, K. Zhu¹, K. J. Zhu^{1,53,58}, L. X. Zhu⁵⁸, S. H. Zhu⁶⁵, S. Q. Zhu³⁸, T. J. Zhu⁷², W. J. Zhu^{10,f}, Y. C. Zhu^{66,53}, Z. A. Zhu^{1,58}, B. S. Zou¹, J. H. Zou¹

(BESIII Collaboration)

- ¹ Institute of High Energy Physics, Beijing 100049, People's Republic of China
² Beihang University, Beijing 100191, People's Republic of China
³ Beijing Institute of Petrochemical Technology, Beijing 102617, People's Republic of China
⁴ Bochum Ruhr-University, D-44780 Bochum, Germany
⁵ Carnegie Mellon University, Pittsburgh, Pennsylvania 15213, USA
⁶ Central China Normal University, Wuhan 430079, People's Republic of China
⁷ Central South University, Changsha 410083, People's Republic of China
⁸ China Center of Advanced Science and Technology, Beijing 100190, People's Republic of China
⁹ COMSATS University Islamabad, Lahore Campus, Defence Road, Off Raiwind Road, 54000 Lahore, Pakistan
¹⁰ Fudan University, Shanghai 200433, People's Republic of China
¹¹ G.I. Budker Institute of Nuclear Physics SB RAS (BINP), Novosibirsk 630090, Russia
¹² GSI Helmholtzcentre for Heavy Ion Research GmbH, D-64291 Darmstadt, Germany
¹³ Guangxi Normal University, Guilin 541004, People's Republic of China
¹⁴ Guangxi University, Nanning 530004, People's Republic of China
¹⁵ Hangzhou Normal University, Hangzhou 310036, People's Republic of China
¹⁶ Hebei University, Baoding 071002, People's Republic of China
¹⁷ Helmholtz Institute Mainz, Staudinger Weg 18, D-55099 Mainz, Germany
¹⁸ Henan Normal University, Xinxiang 453007, People's Republic of China
¹⁹ Henan University of Science and Technology, Luoyang 471003, People's Republic of China
²⁰ Henan University of Technology, Zhengzhou 450001, People's Republic of China
²¹ Huangshan College, Huangshan 245000, People's Republic of China
²² Hunan Normal University, Changsha 410081, People's Republic of China
²³ Hunan University, Changsha 410082, People's Republic of China
²⁴ Indian Institute of Technology Madras, Chennai 600036, India
²⁵ Indiana University, Bloomington, Indiana 47405, USA
²⁶ INFN Laboratori Nazionali di Frascati, (A)INFN Laboratori Nazionali di Frascati, I-00044, Frascati, Italy; (B)INFN Sezione di Perugia, I-06100, Perugia, Italy; (C)University of Perugia, I-06100, Perugia, Italy
²⁷ INFN Sezione di Ferrara, (A)INFN Sezione di Ferrara, I-44122, Ferrara, Italy; (B)University of Ferrara, I-44122, Ferrara, Italy
²⁸ Institute of Modern Physics, Lanzhou 730000, People's Republic of China
²⁹ Institute of Physics and Technology, Peace Ave. 54B, Ulaanbaatar 13330, Mongolia
³⁰ Jilin University, Changchun 130012, People's Republic of China
³¹ Johannes Gutenberg University of Mainz, Johann-Joachim-Becher-Weg 45, D-55099 Mainz, Germany
³² Joint Institute for Nuclear Research, 141980 Dubna, Moscow region, Russia
³³ Justus-Liebig-Universität Giessen, II. Physikalisches Institut, Heinrich-Buff-Ring 16, D-35392 Giessen, Germany
³⁴ Lanzhou University, Lanzhou 730000, People's Republic of China
³⁵ Liaoning Normal University, Dalian 116029, People's Republic of China
³⁶ Liaoning University, Shenyang 110036, People's Republic of China
³⁷ Nanjing Normal University, Nanjing 210023, People's Republic of China
³⁸ Nanjing University, Nanjing 210093, People's Republic of China
³⁹ Nankai University, Tianjin 300071, People's Republic of China
⁴⁰ National Centre for Nuclear Research, Warsaw 02-093, Poland
⁴¹ North China Electric Power University, Beijing 102206, People's Republic of China
⁴² Peking University, Beijing 100871, People's Republic of China
⁴³ Qufu Normal University, Qufu 273165, People's Republic of China
⁴⁴ Shandong Normal University, Jinan 250014, People's Republic of China
⁴⁵ Shandong University, Jinan 250100, People's Republic of China
⁴⁶ Shanghai Jiao Tong University, Shanghai 200240, People's Republic of China
⁴⁷ Shanxi Normal University, Linfen 041004, People's Republic of China
⁴⁸ Shanxi University, Taiyuan 030006, People's Republic of China
⁴⁹ Sichuan University, Chengdu 610064, People's Republic of China
⁵⁰ Soochow University, Suzhou 215006, People's Republic of China
⁵¹ South China Normal University, Guangzhou 510006, People's Republic of China
⁵² Southeast University, Nanjing 211100, People's Republic of China
⁵³ State Key Laboratory of Particle Detection and Electronics, Beijing 100049, Hefei 230026, People's Republic of China

- ⁵⁴ Sun Yat-Sen University, Guangzhou 510275, People's Republic of China
- ⁵⁵ Suranaree University of Technology, University Avenue 111, Nakhon Ratchasima 30000, Thailand
- ⁵⁶ Tsinghua University, Beijing 100084, People's Republic of China
- ⁵⁷ Turkish Accelerator Center Particle Factory Group, (A)Istinye University, 34010, Istanbul, Turkey; (B)Near East University, Nicosia, North Cyprus, Mersin 10, Turkey
- ⁵⁸ University of Chinese Academy of Sciences, Beijing 100049, People's Republic of China
- ⁵⁹ University of Groningen, NL-9747 AA Groningen, The Netherlands
- ⁶⁰ University of Hawaii, Honolulu, Hawaii 96822, USA
- ⁶¹ University of Jinan, Jinan 250022, People's Republic of China
- ⁶² University of Manchester, Oxford Road, Manchester, M13 9PL, United Kingdom
- ⁶³ University of Muenster, Wilhelm-Klemm-Str. 9, 48149 Muenster, Germany
- ⁶⁴ University of Oxford, Keble Rd, Oxford, UK OX13RH
- ⁶⁵ University of Science and Technology Liaoning, Anshan 114051, People's Republic of China
- ⁶⁶ University of Science and Technology of China, Hefei 230026, People's Republic of China
- ⁶⁷ University of South China, Hengyang 421001, People's Republic of China
- ⁶⁸ University of the Punjab, Lahore-54590, Pakistan
- ⁶⁹ University of Turin and INFN, (A)University of Turin, I-10125, Turin, Italy; (B)University of Eastern Piedmont, I-15121, Alessandria, Italy; (C)INFN, I-10125, Turin, Italy
- ⁷⁰ Uppsala University, Box 516, SE-75120 Uppsala, Sweden
- ⁷¹ Wuhan University, Wuhan 430072, People's Republic of China
- ⁷² Xinyang Normal University, Xinyang 464000, People's Republic of China
- ⁷³ Yunnan University, Kunming 650500, People's Republic of China
- ⁷⁴ Zhejiang University, Hangzhou 310027, People's Republic of China
- ⁷⁵ Zhengzhou University, Zhengzhou 450001, People's Republic of China
- ^a Also at the Moscow Institute of Physics and Technology, Moscow 141700, Russia
- ^b Also at the Novosibirsk State University, Novosibirsk, 630090, Russia
- ^c Also at the NRC "Kurchatov Institute", PNPI, 188300, Gatchina, Russia
- ^d Also at Goethe University Frankfurt, 60323 Frankfurt am Main, Germany
- ^e Also at Key Laboratory for Particle Physics, Astrophysics and Cosmology, Ministry of Education; Shanghai Key Laboratory for Particle Physics and Cosmology; Institute of Nuclear and Particle Physics, Shanghai 200240, People's Republic of China
- ^f Also at Key Laboratory of Nuclear Physics and Ion-beam Application (MOE) and Institute of Modern Physics, Fudan University, Shanghai 200443, People's Republic of China
- ^g Also at State Key Laboratory of Nuclear Physics and Technology, Peking University, Beijing 100871, People's Republic of China
- ^h Also at School of Physics and Electronics, Hunan University, Changsha 410082, China
- ⁱ Also at Guangdong Provincial Key Laboratory of Nuclear Science, Institute of Quantum Matter, South China Normal University, Guangzhou 510006, China
- ^j Also at Frontiers Science Center for Rare Isotopes, Lanzhou University, Lanzhou 730000, People's Republic of China
- ^k Also at Lanzhou Center for Theoretical Physics, Lanzhou University, Lanzhou 730000, People's Republic of China
- ^l Also at the Department of Mathematical Sciences, IBA, Karachi, Pakistan

We report a measurement of the cross section for the process $e^+e^- \rightarrow \pi^+\pi^-J/\psi$ around the $X(3872)$ mass in search for the direct formation of $e^+e^- \rightarrow X(3872)$ through the two-photon fusion process. No enhancement of the cross section is observed at the $X(3872)$ peak and an upper limit on the product of electronic width and branching fraction of $X(3872) \rightarrow \pi^+\pi^-J/\psi$ is determined to be $\Gamma_{ee} \times \mathcal{B}(X(3872) \rightarrow \pi^+\pi^-J/\psi) < 7.5 \times 10^{-3}$ eV at 90% confidence level under an assumption of total width of 1.19 ± 0.21 MeV. This is an improvement of a factor of about 17 compared to the previous limit. Furthermore, using the latest result of $\mathcal{B}(X(3872) \rightarrow \pi^+\pi^-J/\psi)$, an upper limit on the electronic width Γ_{ee} of $X(3872)$ is obtained to be < 0.32 eV at the 90% confidence level.

PACS numbers: 13.66.Bc, 14.40.Gx

I. INTRODUCTION

The observation of the $X(3872)$ state ¹ by the Belle collaboration in 2003 [1] and its confirmation by other

experiments [2–7] opened a new field of charmonium-like exotic states. Being difficult to fit into the conventional charmonium spectrum [8, 9], the XYZ states are candidates for tetraquarks, meson molecules, hybrid mesons, and kinematic effects [9–11]. The $X(3872)$ state is probably the best known representative of these states. It has been observed in B decays, in radiative transitions of the $Y(4260)$ resonance, as well as in inclusive pp and $p\bar{p}$ col-

¹ also called $\chi_{c1}(3872)$, according to its quantum numbers

lisions [12]. Up to now, its decays into six different final states are established [12–14]. Its mass is very close to the threshold of $D\bar{D}^*$ production, which also represents one of its largest decay modes. This property leads naturally to the hypothesis that it is a meson molecule [10, 15]. One important discriminant between different models is the $X(3872)$ width. Recently, two new measurements of its width were reported by the LHCb experiment [16, 17], and an average of 1.19 ± 0.21 MeV based on these two new measurements is reported in Ref. [12].

The quantum numbers J^{PC} of the $X(3872)$ state are measured to be 1^{++} [18], which allows suppressed formation in e^+e^- collisions via two-photon fusion [19, 20]. Recently, a search for the $X(3872)$ in two-photon interactions in the process of $e^+e^- \rightarrow e^+e^-\pi^+\pi^-J/\psi$ was reported by the BELLE collaboration and evidence of $X(3872)$ production is found [21]. Furthermore, the BESIII collaboration recently reported the first observation of the 1^{++} state χ_{c1} in direct e^+e^- annihilation with a significance of 5.1σ [22]. These findings motivate the search for direct formation of $X(3872)$ via the two photon fusion process in e^+e^- annihilation. Furthermore, knowledge of the electronic width Γ_{ee} might help to reveal the nature of $X(3872)$. The current upper limit is $\Gamma_{ee} \times \mathcal{B}(X(3872) \rightarrow \pi^+\pi^-J/\psi) < 0.13$ eV at the 90% confidence level (C.L.), determined by BESIII via the initial-state radiation (ISR) process [23]. A theoretical prediction using vector meson dominance yields $\Gamma_{ee} \gtrsim 0.03$ eV and a lower bound of $\Gamma_{ee} \times \mathcal{B}(X(3872) \rightarrow \pi^+\pi^-J/\psi) \gtrsim 0.96 \times 10^{-3}$ eV [24].

In this paper, the cross section $\sigma(e^+e^- \rightarrow \pi^+\pi^-J/\psi)$ around the $X(3872)$ mass is measured to search for the direct production of $X(3872)$ and measure the electronic width of $X(3872)$ using data sets collected by the BESIII detector. Two processes are considered, the non-resonant continuum process and the resonant signal process via two-photon fusion as shown in Fig. 1. An enhanced cross section is expected at the $X(3872)$ peak over the off-resonance region if the direct production process is significant.

II. BESIII DETECTOR AND DATA SAMPLES

The BESIII detector [26] records symmetric e^+e^- collisions provided by the BEPCII storage ring, which operates with a peak luminosity of 1×10^{33} $\text{cm}^{-2}\text{s}^{-1}$ at the center-of-mass (c.m.) energy of $\sqrt{s} = 3.89$ GeV. The cylindrical core of the BESIII detector covers 93% of the full solid angle and consists of a helium-based multilayer drift chamber (MDC), a plastic scintillator time-of-flight system (TOF), and a CsI(Tl) electromagnetic calorimeter (EMC), which are all enclosed in a superconducting solenoidal magnet providing a 1.0 T (0.9 T in 2012) magnetic field. The solenoid is supported by an octagonal flux-return yoke with resistive-plate-counter modules interleaved with steel, which are used for muon identification. The charged-particle momentum resolution at

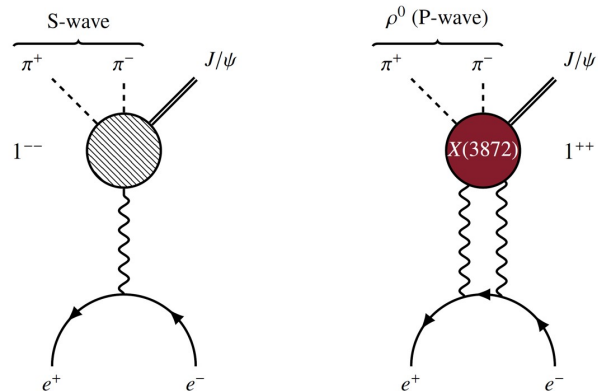


FIG. 1. Feynman diagrams of the non-resonant continuum process $e^+e^- \rightarrow \pi^+\pi^-J/\psi$ (left) and the resonant signal process $e^+e^- \rightarrow X(3872) \rightarrow \pi^+\pi^-J/\psi$ (right), of which it is known that the $\pi^+\pi^-$ pair forms a ρ^0 meson [6, 18, 25].

1 GeV/c is 0.5%, and the specific energy loss (dE/dx) resolution is 6% for electrons from Bhabha scattering. The EMC measures photon energies with a resolution of 2.5% (5%) at 1 GeV in the barrel (end-cap) region. The time resolution in the TOF barrel region is 68 ps, while that in the end-cap region is 110 ps. The end-cap TOF system was upgraded in 2015 using multi-gap resistive plate chambers, providing a time resolution of 60 ps [27–29].

In this work, four data sets collected by the BESIII detector are used. Among the four data sets, two dedicated data sets were recorded in the vicinity of the $X(3872)$ mass, one directly on the $X(3872)$ peak with c.m. energy of 3871.3 MeV (on-resonance) and with a luminosity of 110.3 pb^{-1} , and the other one about 4 MeV below the peak at 3867.4 MeV (off-resonance) and with a luminosity of 108.9 pb^{-1} . For these two dedicated data sets, a Beam Energy Measurement System (BEMS) [30] provides the realtime measurement of the c.m. energy with an uncertainty smaller than 100 keV and of the energy spread with an uncertainty smaller than 200 keV. The resolution of c.m. energy from BEMS is smaller than the width of $X(3872)$, and far smaller than the 4 MeV energy difference between the on-resonance and off-resonance data sets. This ensures a negligible fraction of resonant contribution in the off-resonance data set at 3867.4 MeV. Two further off-resonance data sets at 3807.7 (50.5 pb^{-1}) and 3896.2 (52.6 pb^{-1}) MeV are used [31]. The luminosity of all data sets are determined by the analysis of large-angle Bhabha scattering events.

Simulated data samples produced with a GEANT4-based [32] Monte Carlo (MC) package, which includes the geometric description of the BESIII detector and the detector response, are used to determine detection efficiencies and to estimate backgrounds. The simulation models the beam energy spread and initial state radiation (ISR) in the e^+e^- annihilations with the generator KKMC [33]. For each of the four different data sam-

ples, 5×10^5 signal MC events with $J/\psi \rightarrow e^+e^-$ and 5×10^5 signal MC events with $J/\psi \rightarrow \mu^+\mu^-$ are simulated with different models including VVPIPI and σ PHSP [34]. The VVPIPI model describes the decay of a vector state to a vector state and $\pi^+\pi^-$ where the $\pi^+\pi^-$ system is dominated by a S-wave. The σ PHSP is a model with phase space decay of $e^+e^- \rightarrow \sigma J/\psi$ and $\sigma \rightarrow \pi^+\pi^-$. To estimate the background contamination from non- $\pi^+\pi^- J/\psi$ events, background MC samples are generated, including $e^+e^- \rightarrow \gamma e^+e^-$, $\gamma\mu^+\mu^-$, $e^+e^-e^+e^-$, $e^+e^-\mu^+\mu^-$, $e^+e^-q\bar{q}$, $\pi^+\pi^-\pi^+\pi^-$, $K_S^0 K^\pm \pi^\mp$, $K^+K^-\pi^+\pi^-$, and $e^+e^- \rightarrow \gamma_{\text{ISR}}\psi' \rightarrow \gamma_{\text{ISR}}\pi^+\pi^- J/\psi \rightarrow \gamma_{\text{ISR}}\pi^+\pi^-\ell^+\ell^-$. These backgrounds are scaled to the integrated luminosity of data for each energy point.

III. EVENT SELECTION

In the process of $e^+e^- \rightarrow \pi^+\pi^- J/\psi$, J/ψ is reconstructed via its decay to lepton pairs $\ell^+\ell^-$ ($\ell = e, \mu$). The final state $\pi^+\pi^-\ell^+\ell^-$ consists of four charged tracks with zero net charge. The lepton tracks coming from the J/ψ decay have larger momenta (in the lab frame) compared to the pion tracks. Tracks with momenta lower than 0.6 GeV/c are assumed to be pion candidates and lepton candidates are required to have momenta larger than 1.0 GeV/c. Each candidate event is required to have two pion candidates and two lepton candidates, both having opposite charges. The J/ψ decay modes can be distinguished by the energy deposition in the EMC associated to the lepton tracks. Electrons deposit a large fraction of their energy, while the muons pass through the EMC leaving only a small energy deposition. The deposited energy in EMC is required to be smaller than 0.35 GeV for both muons and larger than 1.1 GeV for both electrons. Each event is required to have either two electron candidates or two muon candidates.

Candidate events of $e^+e^- \rightarrow \pi^+\pi^-\ell^+\ell^-$ are subjected to a kinematic fit with four constraints (4C) on the energy-momentum of the final states. The chi-square of kinematic fit, χ_{4C}^2 , is required to be smaller than 60. To remove photon conversion background, which could be misidentified as a $\pi^+\pi^-$ pair or $\pi^\pm e^\mp$, requirements of $\cos\theta_{\pi^+\pi^-} < 0.95$ and $\cos\theta_{\pi^\pm e^\mp} < 0.98$ are applied. Here, $\theta_{\pi^+\pi^-}$ is the opening angle between the two pion candidates, and $\theta_{\pi^\pm e^\mp}$ is the opening angle between the pion and oppositely charged electron candidates.

The invariant mass distributions of the di-lepton pairs that pass all selection criteria are shown in Fig. 2. Here, the four data sets are combined together. The J/ψ peak is clearly visible, and the peak region $m(\ell^+\ell^-) \in [3.08, 3.12]$ GeV/c² is indicated by a pair of black arrows as well as the sideband region $m(\ell^+\ell^-) \in [3.02, 3.06]$ or $[3.14, 3.18]$ GeV/c² (gray arrows). In order to estimate the background contamination from non- $\pi^+\pi^- J/\psi$ events, the backgrounds $e^+e^- \rightarrow \gamma e^+e^-$, $\gamma\mu^+\mu^-$, $e^+e^-e^+e^-$, $e^+e^-\mu^+\mu^-$, $e^+e^-q\bar{q}$, $\pi^+\pi^-\pi^+\pi^-$, $K_S^0 K^\pm \pi^\mp$, $K^+K^-\pi^+\pi^-$ were simulated. For the e^+e^- mode, the

background MC fails to describe the data. However, no peaking background is found from the simulation. This motivates an estimation of the background contamination by J/ψ sidebands.

The number of signal events is determined from the J/ψ peak. Instead of using the $\ell^+\ell^-$ invariant mass after the kinematic fit, the recoil mass of the two pions before the fit is used due to a better resolution. Independent unbinned maximum likelihood fits to the recoil mass of the two pions are performed for both J/ψ decay modes in the range of $m(\ell^+\ell^-) \in [3.0, 3.2]$ GeV/c². In the fit, the signal is described with a line shape derived from MC simulation, while the background is modeled as a linear function.

IV. RESULTS

The cross section of the process $e^+e^- \rightarrow \pi^+\pi^- J/\psi$ is determined using

$$\sigma = \frac{N_{\text{obs}}}{\int \mathcal{L} dt \cdot \epsilon \cdot (1 + \delta) \cdot \mathcal{B}(J/\psi \rightarrow \ell^+\ell^-)}. \quad (1)$$

Here, N_{obs} is the number of observed signal events, $\int \mathcal{L} dt$ is the integrated luminosity, ϵ is the detection efficiency determined from MC samples, and $(1 + \delta)$ is the radiative correction factor to account for ISR. It is calculated using the KKMC event generator with the input line-shape updated iteratively until it converges.

Table I shows the measured cross sections at the four energy points with two J/ψ modes. The cross sections with two J/ψ modes combined are also listed in Table I where the uncertainties are only statistical. In Fig. 3, the cross sections are plotted with the systematic uncertainties which will be described later. In the plot, the dashed vertical line indicates the location of the $X(3872)$ peak. The dot-dashed curve shows the line-shape assuming a total width of 1.19 MeV and $\Gamma_{ee} \times \mathcal{B}(X(3872) \rightarrow \pi^+\pi^- J/\psi) = 0.013$ eV. There is no interference between the resonant and continuum parts due to their different quantum numbers. The value of 0.013 eV is arbitrarily chosen as one order of magnitude lower than the previous upper limit [23], and only for illustration purposes. From these data points, no enhancement of the cross section is observed at the $X(3872)$ peak. The cross section on-resonance is smaller than that of the off-resonance region, which can be observed as a dip in Fig. 3. Given the low statistics, the dip is insignificant and consistent with a flat distribution within 1σ .

To interpret the cross section, the two processes in Fig. 1 are considered. Due to the different quantum numbers of the final state in continuum process and the resonant $X(3872)$ formation, the total $e^+e^- \rightarrow \pi^+\pi^- J/\psi$ cross section is modeled as an incoherent sum of the two processes. The cross section from continuum is assumed to be a linear function of c.m. energy. The $X(3872)$ is modeled as a relativistic Breit-Wigner resonance. Only

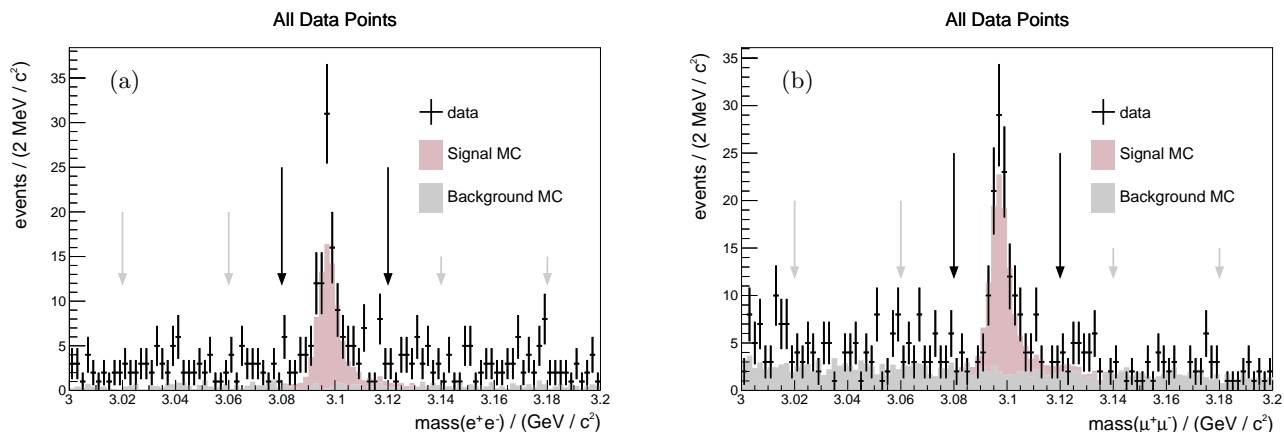


FIG. 2. Comparison between data, signal MC, and background MC distributions of $m(\ell^+\ell^-)$. All four data sets are combined. The MC distributions are scaled to match the integrated luminosity of the data. The black (gray) arrows indicate the peak (sideband) region.

the $\pi^+\pi^-J/\psi$ decay mode is reconstructed in the cross section measurement. As a consequence, the corresponding branching fraction needs to be included in the line-shape parameterization:

$$\sigma(\sqrt{s}) = \sigma_{\text{cont}} + 12\pi \frac{\Gamma_{\text{tot}}\Gamma_{ee} \times \mathcal{B}(X(3872) \rightarrow \pi^+\pi^-J/\psi)}{(s - m_0^2)^2 + m_0^2\Gamma_{\text{tot}}^2}, \quad (2)$$

where σ_{cont} , Γ_{tot} , and Γ_{ee} are the constant continuum cross section, the total width and the electronic width of the $X(3872)$, respectively. m_0 is the mass of $X(3872)$.

In 2020, two measurements on the total width were released as $(1.39 \pm 0.24 \pm 0.10)$ MeV [16] and $(0.96_{-0.18}^{+0.19} \pm 0.21)$ MeV [17], resulting in an average value of (1.19 ± 0.21) MeV [12]. In this analysis, we treat the product $\Gamma_{ee} \times \mathcal{B}(X(3872) \rightarrow \pi^+\pi^-J/\psi)$ as one parameter, and an upper limit on this product is measured. Then, we also calculate Γ_{ee} using two different values for the branching fraction $\mathcal{B}(X(3872) \rightarrow \pi^+\pi^-J/\psi)$. This was recently measured to be $(4.1 \pm 1.3)\%$ by the BABAR collaboration [35], and the latest world average value is $(3.8 \pm 1.2)\%$ [12].

In total, there are three unknown parameters left, σ_{cont} , Γ_{tot} , and $\Gamma_{ee} \times \mathcal{B}(X(3872) \rightarrow \pi^+\pi^-J/\psi)$ or Γ_{ee} . The mass m_0 is fixed to (3871.65 ± 0.06) MeV/ c^2 [12]. Using the line-shape parameterization, an extended likelihood function depending on the cross section for each data set and J/ψ mode is constructed. Upper limits for the electronic width are determined at different Γ_{tot} inputs. Figure 4 shows the determination of the upper limit on $\Gamma_{ee} \times \mathcal{B}$ for an assumed total width of 1.19 MeV. Figure 5 shows a scan of $\Gamma_{ee} \times \mathcal{B}$ in a wide range of Γ_{tot} from 0 to 3 MeV. Four different Γ_{tot} , [0.96 [17], 1.19 [12], <1.2 [12], 1.39 [16]] MeV, are indicated with vertical lines. For each of the Γ_{tot} inputs with a mean value and an uncertainty, a unique value of the upper

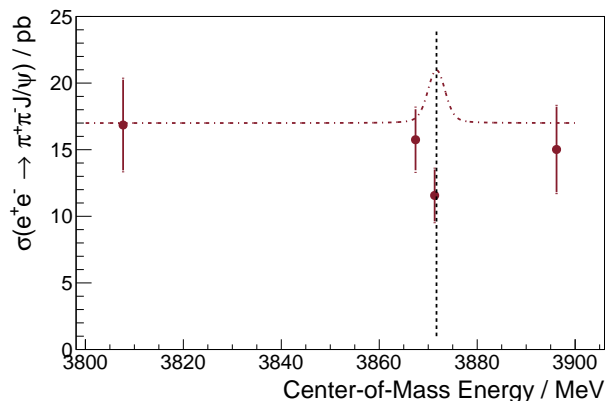


FIG. 3. Cross section of $e^+e^- \rightarrow \pi^+\pi^-J/\psi$. The results of both J/ψ decay modes are combined. The error bars represent the total uncertainties, *i.e.*, the quadratic sum of the statistical and systematic uncertainties. The dashed vertical line indicates the peak position of $X(3872)$. The dot-dashed curve shows an illustration of expected line-shape assuming $\Gamma_{ee} \times \mathcal{B}(X(3872) \rightarrow \pi^+\pi^-J/\psi) = 0.013$ eV.

limit of $\Gamma_{ee} \times \mathcal{B}$ is obtained by an integral of the likelihood over Γ_{tot} based on a Gaussian assumption of Γ_{tot} . These upper limits are shown in Table II, where both the statistical and systematic uncertainties have been considered.

V. SYSTEMATIC UNCERTAINTIES

There are two different kinds of systematic uncertainties that have to be treated separately. Uncertainties of the first kind affect the cross section measurement; they comprise the uncertainty of the integrated luminosity, the tracking efficiency, the branching fraction of J/ψ decays

TABLE I. Result of the fit to the dilepton mass distribution. Shown are the results of the two independent J/ψ modes and a combined value. The uncertainties are only statistical.

\sqrt{s}/MeV	3807.7 ± 0.6	3867.408 ± 0.031	3871.31 ± 0.06	3896.2 ± 0.8
$\int \mathcal{L} dt / \text{pb}^{-1}$	50.5 ± 0.5	108.9 ± 1.3	110.3 ± 0.8	52.6 ± 0.5
$(1 + \delta)$	0.895	0.895	0.895	0.895
$N_{obs}^{e^+e^-}$	19 ± 5	30 ± 7	24 ± 6	16 ± 5
$\epsilon^{e^+e^-} / \%$	31.78 ± 0.08	31.34 ± 0.08	31.29 ± 0.08	31.68 ± 0.08
$\sigma^{e^+e^-} / \text{pb}$	22.0 ± 6.4	16.4 ± 3.6	12.7 ± 3.3	17.0 ± 5.2
$N_{obs}^{\mu^+\mu^-}$	18 ± 5	40 ± 8	29 ± 6	17 ± 5
$\epsilon^{\mu^+\mu^-} / \%$	45.38 ± 0.10	44.90 ± 0.09	44.72 ± 0.09	45.14 ± 0.10
$\sigma^{\mu^+\mu^-} / \text{pb}$	14.8 ± 4.0	15.3 ± 2.9	10.9 ± 2.4	13.4 ± 4.1
$\sigma^{\ell^+\ell^-} / \text{pb}$	16.9 ± 3.4	15.7 ± 2.3	11.6 ± 1.9	15.0 ± 3.2

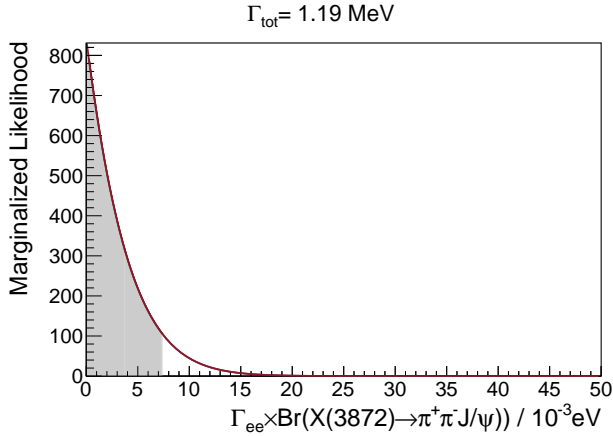


FIG. 4. Determination of the upper limit on $\Gamma_{ee} \times \mathcal{B}$ for an assumed total width of 1.19 MeV. The gray area indicates the 90% integral. The value of $\Gamma_{ee} \times \mathcal{B}$ at the right edge of that area is the upper limit on $\Gamma_{ee} \times \mathcal{B}$ at the 90% confidence level.

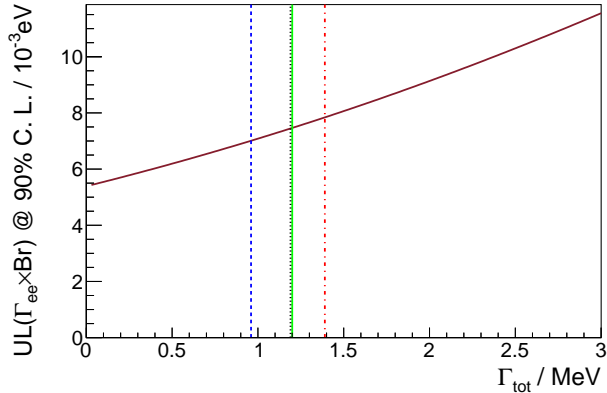


FIG. 5. Upper limit on $\Gamma_{ee} \times \mathcal{B}$ at the 90% confidence level as a function of the total width. The vertical lines indicates four different values of Γ_{tot} , [0.96 [17], 1.19 [12], <1.2 [12], 1.39 [16]] MeV.

TABLE II. Γ_{ee} and $\Gamma_{ee} \times \mathcal{B}(X(3872) \rightarrow \pi^+\pi^-J/\psi)$, using different values for the $X(3872)$ total width of (0.96 ± 0.21) MeV [17], (1.19 ± 0.21) MeV [12], (1.39 ± 0.24) MeV [16], and the current upper limit of 1.2 MeV [12]. Two input values for $\mathcal{B}(X(3872) \rightarrow \pi^+\pi^-J/\psi)$ are used, $\mathcal{B}_1 = (4.1 \pm 1.3)\%$ [35], and $\mathcal{B}_2 = (3.8 \pm 1.2)\%$.

$\Gamma_{tot} / \text{MeV}$	$\Gamma_{ee} / 10^{-3} \text{ eV}$		$\Gamma_{ee} \times \mathcal{B} / 10^{-3} \text{ eV}$
	\mathcal{B}_1	\mathcal{B}_2	—
0.96 ± 0.21	< 293	< 305	< 7.0
1.19 ± 0.21	< 309	< 322	< 7.5
1.39 ± 0.24	< 324	< 338	< 7.9
< 1.2	< 270	< 282	< 6.5

to lepton pairs, the line-shape of the continuum process, the kinematic fit, the decay model, the fit to the invariant mass of J/ψ , and the resolution of the invariant mass of lepton pair.

The integrated luminosity is determined using the same strategy as in Ref. [31]. The uncertainty of the tracking efficiency is 1% per track yielding a 4% uncertainty [36]. The uncertainty from the line-shape of the continuum process is estimated by changing the assumed flat distribution to be the line-shape reported in Ref. [37]. In the kinematic fits, the helix parameters of charged tracks are corrected to reduce the discrepancy between data and MC simulation as described in Ref. [38]. The difference between MC samples with and without the correction is taken as the uncertainty from the kinematic fits. The uncertainty associated with the decay model is estimated by the efficiency difference between σ PHSP model and VVPIPI model [34]. In the fit to the $m(\ell^+\ell^-)$ distribution, the background is modeled as a linear function. To estimate the uncertainty from the background modeling in the fit, an alternative fit using a quadratic function is performed to 1000 pseudo data sets. These pseudo data sets are sampled from the real data using a bootstrap method, where the events from the real data are allowed to be picked multiple times. The fit results are averaged and the difference to the nominal fit is taken as systematic uncertainty associated with the fit. In order to account for the difference of the resolution of

$m(\ell^+\ell^-)$ in data and simulation, an alternative fit to the $m(\ell^+\ell^-)$ spectrum is performed. The signal probability density function is convolved with a Gaussian and the resulting difference in $\sigma(e^+e^- \rightarrow \pi^+\pi^- J/\psi)$ is less than 0.1% and can be neglected. These systematic uncertainties are summarized in Table III.

Uncertainties of the second kind affect the line-shape parameterization. They include the uncertainties associated with the $X(3872)$ mass, \sqrt{s} , and the beam energy spread. The values for these parameters are sampled from the corresponding distributions to calculate the likelihood. With a subsequent integral over the likelihood, these uncertainties have already been included in the electronic width measurement.

VI. SUMMARY

In summary, the cross sections of the process $e^+e^- \rightarrow \pi^+\pi^- J/\psi$ are measured at four different c.m. energies around the $X(3872)$ mass. The results of these measurements are listed in Table I. Since the direct production of the $X(3872)$ is not observed, an upper limit on $\Gamma_{ee} \times \mathcal{B}$ is determined. For an assumed total width of 1.19 ± 0.21 MeV, the upper limit on $\Gamma_{ee} \times \mathcal{B}$ is determined to be 7.5×10^{-3} eV at the 90% C.L., with an improvement of a factor of about 17 compared to the previous limit [23]. The upper limits on $\Gamma_{ee} \times \mathcal{B}$ are also calculated for other values of Γ_{tot} , as summarized in Table II. There is no conflict to the theoretical prediction of $\Gamma_{ee} \times \mathcal{B} \gtrsim 0.96 \times 10^{-3}$ eV [24]. Using the recently released measurements of $\mathcal{B}(X(3872) \rightarrow \pi^+\pi^- J/\psi)$, an upper limit on Γ_{ee} is reported for the first time.

ACKNOWLEDGMENTS

The BESIII collaboration thanks the staff of BEPCII and the IHEP computing center for their strong sup-

port. This work is supported in part by National Natural Science Foundation of China (NSFC) under Contracts Nos. 11975278, 11635010, 11735014, 11835012, 11935015, 11935016, 11935018, 11961141012, 12022510, 12025502, 12035009, 12035013, 12192260, 12192261, 12192262, 12192263, 12192264, 12192265; National Key Research and Development Program of China under Contracts Nos. 2020YFA0406300, 2020YFA0406400; the Chinese Academy of Sciences (CAS) Large-Scale Scientific Facility Program; Joint Large-Scale Scientific Facility Funds of the NSFC and CAS under Contracts Nos. U2032105, U2032109, U1832207; CAS Key Research Program of Frontier Sciences under Contract No. QYZDJ-SSW-SLH040; 100 Talents Program of CAS; CAS Interdisciplinary Innovation Team; Key Research Program of the Chinese Academy of Sciences under Contract No. XDB34030301; INPAC and Shanghai Key Laboratory for Particle Physics and Cosmology; ERC under Contract No. 758462; European Union's Horizon 2020 research and innovation programme under Marie Skłodowska-Curie grant agreement under Contract No. 894790; German Research Foundation DFG under Contracts Nos. 443159800, Collaborative Research Center CRC 1044, GRK 2149; Istituto Nazionale di Fisica Nucleare, Italy; Ministry of Development of Turkey under Contract No. DPT2006K-120470; National Science and Technology fund; National Science Research and Innovation Fund (NSRF) via the Program Management Unit for Human Resources and Institutional Development, Research and Innovation under Contract No. B16F640076; STFC (United Kingdom); Suranaree University of Technology (SUT), Thailand Science Research and Innovation (TSRI), and National Science Research and Innovation Fund (NSRF) under Contract No. 160355; The Royal Society, UK under Contracts Nos. DH140054, DH160214; The Swedish Research Council; U. S. Department of Energy under Contract No. DE-FG02-05ER41374.

-
- [1] S. K. Choi *et al.* (Belle Collaboration), *Phys. Rev. Lett.* **91**, 262001 (2003).
 - [2] B. Aubert *et al.* (BABAR Collaboration), *Phys. Rev. D* **71**, 071103 (2005).
 - [3] D. Acosta *et al.* (CDF II Collaboration), *Phys. Rev. Lett.* **93**, 072001 (2004).
 - [4] V. M. Abazov *et al.* (D0 Collaboration), *Phys. Rev. Lett.* **93**, 162002 (2004).
 - [5] R. Aaij *et al.* (LHCb Collaboration), *Eur. Phys. J. C* **72**, 1972 (2012).
 - [6] S. Chatrchyan *et al.* (CMS Collaboration), *J. High Energ. Phys.* **2013**, 154.
 - [7] M. Ablikim *et al.* (BESIII Collaboration), *Phys. Rev. Lett.* **112**, 092001 (2014).
 - [8] S. Godfrey and N. Isgur, *Phys. Rev. D* **32**, 189 (1985).
 - [9] R. F. Lebed, R. E. Mitchell, and E. S. Swanson, *Prog. Part. Nucl. Phys.* **93**, 143 (2017).
 - [10] F.-K. Guo, C. Hanhart, U.-G. Meißner, Q. Wang, Q. Zhao, and B.-S. Zou, *Rev. Mod. Phys.* **90**, 015004 (2018).
 - [11] A. Ali, J. S. Lange, and S. Stone, *Prog. Part. Nucl. Phys.* **97**, 123 (2017).
 - [12] P. A. Zyla *et al.* (Particle Data Group), *Prog. Theor. Exp. Phys.* **2020**, 083C01 (2020), and 2021 update.
 - [13] M. Ablikim *et al.* (BESIII Collaboration), *Phys. Rev. Lett.* **122**, 202001 (2019).
 - [14] C. Li and C.-Z. Yuan, *Phys. Rev. D* **100**, 094003 (2019).
 - [15] E. Braaten and M. Kusunoki, *Phys. Rev. D* **69**, 074005 (2004).
 - [16] R. Aaij *et al.* (LHCb Collaboration), *Phys. Rev. D* **102**, 092005 (2020).
 - [17] R. Aaij *et al.* (LHCb Collaboration), *J. High Energ. Phys.* **08**, 123.

TABLE III. Relative systematic uncertainties (in %) on the measured cross section $\sigma(e^+e^- \rightarrow \pi^+\pi^- J/\psi)$. The total uncertainty is the quadratic sum of the individual uncertainties.

Source	3807.7 MeV		3867.4 MeV		3871.3 MeV		3896.2 MeV	
	e^+e^-	$\mu^+\mu^-$	e^+e^-	$\mu^+\mu^-$	e^+e^-	$\mu^+\mu^-$	e^+e^-	$\mu^+\mu^-$
$\int \mathcal{L} dt$	1.0		1.2		0.7		1.0	
Tracking	4.0		4.0		4.0		4.0	
$\mathcal{B}(J/\psi \rightarrow \ell^+\ell^-)$	0.5	0.6	0.5	0.6	0.5	0.6	0.5	0.6
Line-shape	0.8	0.8	1.2	1.7	1.3	1.3	0.7	0.6
Kinematic fit	0.9	0.7	0.8	0.7	0.9	0.7	0.9	0.7
Decay model	2.1	3.6	2.7	4.0	2.2	3.7	2.4	4.0
$m(\ell^+\ell^-)$ fit	4.9	1.2	2.2	1.7	4.2	7.7	11.8	4.2
Total	6.8	5.7	5.7	6.3	6.5	9.6	12.8	7.2

- [18] R. Aaij *et al.* (LHCb Collaboration), *Phys. Rev. Lett.* **110**, 222001 (2013).
- [19] J. H. Kühn, J. Kaplan, and E. G. O. Safiani, *Nucl. Phys. B* **157**, 125 (1979).
- [20] J. Kaplan and J. Kühn, *Phys. Lett. B* **78**, 252 (1978).
- [21] Y. Teramoto *et al.* (Belle Collaboration), *Phys. Rev. Lett.* **126**, 122001 (2021).
- [22] M. Ablikim *et al.* (BESIII Collaboration), *Phys. Rev. Lett.* **129**, 122001 (2022).
- [23] M. Ablikim *et al.* (BESIII Collaboration), *Phys. Lett. B* **749**, 414 (2015).
- [24] A. Denig, F.-K. Guo, C. Hanhart, and A. V. Nefediev, *Phys. Lett. B* **736**, 221 (2014).
- [25] S. K. Choi *et al.* (Belle Collaboration), *Phys. Rev. D* **84**, 052004 (2011).
- [26] M. Ablikim *et al.*, *Nucl. Instr. Meth. A* **614**, 345 (2010).
- [27] Y. Guo *et al.*, *Radiat. Det. Tech. Meth.* **1**, 15 (2017).
- [28] X. Li *et al.*, *Radiat. Det. Tech. Meth.* **1**, 13 (2017).
- [29] P. Cao *et al.*, *Nucl. Instr. Meth. A* **953**, 163053 (2020).
- [30] J. Y. Zhang *et al.*, *Chin. Phys. C* **40**, 076001 (2016).
- [31] M. Ablikim *et al.* (BESIII Collaboration), *Chin. Phys. C* **39**, 093001 (2015).
- [32] S. Agostinelli *et al.*, *Nucl. Instr. Meth. A* **506**, 250 (2003).
- [33] S. Jadach, B. Ward, and Z. Was, *Comp. Phys. Comm.* **130**, 260 (2000).
- [34] D. J. Lange, *Nucl. Instr. Meth. A* **462**, 152 (2001).
- [35] J. P. Lees *et al.* (BaBar Collaboration), *Phys. Rev. Lett.* **124**, 152001 (2020).
- [36] M. Ablikim *et al.* (BESIII Collaboration), *Phys. Rev. D* **100**, 051101 (2019).
- [37] M. Ablikim *et al.* (BESIII Collaboration), *Phys. Rev. Lett.* **118**, 092001 (2017).
- [38] M. Ablikim *et al.* (BESIII Collaboration), *Phys. Rev. D* **87**, 012002 (2013).